Design of near-field optical probes with optimal field enhancement by finite difference time domain electromagnetic simulation

John T. Krug II, Erik J. Sánchez, and X. Sunney Xie[a)]
Department of Chemistry and Chemical Biology, Harvard University, Cambridge, Massachusetts 02138

(Received 1 February 2002; accepted 28 March 2002)

We report the three-dimensional electromagnetic simulation of gold nanoparticles with specific geometries as a means to the rational design of apertureless near-field scanning optical microscopy (NSOM) probes. Analytical solutions for field enhancement by spheroidal particles are used to provide physical insight for probe design. These solutions indicate that probes need to be not only sharp, but also finite in length in order to generate the highest field enhancement. Finite difference time domain (FDTD) simulations of gold particles illuminated by near infrared radiation are performed. Field enhancements for right trigonal pyramids are found to be size and wavelength dependent. Furthermore, the enhancements for these pyramidal particles are higher than for similar length conical particles, which in turn perform better than quasi-infinite conical probes. The particles we design with FDTD can be made using current nanofabrication techniques, and therefore hold great promise as apertureless NSOM probes. These right trigonal pyramids are particularly well suited for use in tip enhanced nonlinear optical microscopy or near-field Raman microscopy. [DOI: 10.1063/1.1479723]

I. INTRODUCTION

Optical microscopy is one of the most powerful tools available to the experimental scientist, but its spatial resolution suffers from the fundamental diffraction limit. A means of circumventing the diffraction limit was theoretically posited as early as 1928, when Synge proposed the use of a small aperture in a metallic sheet for optical measurements.[1] This idea was studied in more detail in 1944 by Bethe, who calculated the field distribution around a subwavelength aperture in a conducting screen illuminated by a plane wave.[2] Bethe's calculation was refined in 1950 by Bouwkamp.[3] In these works, it was shown that optical imaging beyond the diffraction limit was possible. This concept was first experimentally realized in 1972 by Ash and co-workers in the microwave regime.[4] Due to the difficulty of nanometer scale fabrication and manipulation, the practical application of this concept to the visible regime was not possible until more recently. In 1984, Pohl *et al.* were able to image a test sample at ~25 nm resolution by using a narrow aperture.[5] Nearly simultaneously, Harootunian *et al.* developed metal coated, tapered micropipettes for near-field scanning optical microscopy (NSOM).[6]

In 1991, Betzig and co-workers pioneered the use of aluminum coated, tapered optical fibers for NSOM.[7] Their approach stimulated a great deal of interest and popularized the practice of generating near-field optical images with an aperture, which extends many optical contrast mechanisms beyond the diffraction limit. The finite skin depth of metals at optical frequencies, however, places a fundamental limit on the spatial resolution obtainable with coated fiber probes. Furthermore, light throughput is proportional to the sixth power of the aperture size,[2] and thus relatively large input powers are necessary for signal generation.[8] High input power exacerbates the problem of probe heating due to light absorption by the aluminum coating.[9,10] Typical aperture NSOM measurements yield resolutions on the order of 50–100 nm,[5,7,8,11] though careful probe fabrication and optimal imaging conditions can generate resolution on the order of ~30 nm.[12] While this is finer resolution than available with far-field microscopy, many applications require resolution on the order of 10 nm. Examples include the study of closely packed chromophoric proteins in biological membranes.[13]

Shortly after the development of the mature aperture NSOM technique, a number of groups began work on means of generating near-field images with apertureless probes. Specht *et al.* demonstrated apertureless near-field optical imaging by scattering surface plasmons with an STM tip as early as 1992.[14] In 1994, Fischer *et al.* demonstrated the use of a gold coated glass tetrahedron for near-field scattering imaging.[15] Similarly, in 1995, both Kawata *et al.* and Zenhausern *et al.* undertook near-field scattering experiments with solid tips.[16,17] In the same vein, the scattering by a small silver particle close to the surface plasmon resonance has been used to probe the magneto optical Kerr effect.[18] Common to all of these studies is the use of a solid probe as a scattering center, and the signal is collected in the far field at the same wavelength as the illuminating source. Recently, this approach has been extended to the infrared region, with the intent to probe vibrational absorption.[19,20] In all of the studies discussed previously, the detected signals are sensitively dependent on the topographic features of the sample,[21] and quantitative understanding of the optical contrast is difficult.

A distinctly different methodology for apertureless NSOM was proposed in 1998 by Novotny *et al.*[22] and experimentally realized in 1999 by Sánchez *et al.*[23] The method is based on the highly enhanced evanescent wave in the vicinity of an illuminated metal tip.[24–26] Instead of using the probe as a scattering center, the apertureless probe is used

a)Author to whom correspondence should be addressed.

as a highly localized excitation source for a particular molecular transition. The spectroscopic response of the sample, such as fluorescence, Raman or nonlinear response, provides an optical signal at a frequency different from that of the excitation, and is detected in the far field.[22,23] Images generated in this fashion are simpler to interpret, in that the signal originates from the sample rather than from the probe. This concept was first clearly experimentally demonstrated by two-photon excited fluorescence with 20 nm resolution.[23]

This tip enhanced nonlinear optical microscopy (TENOM) experiment takes advantage of a very high field enhancement to generate contrast above the far-field background. Similarly, surface enhanced Raman scattering (SERS)[27,28] utilizes high field enhancements to generate strong signals. In fact, extremely strong field enhancement has made possible the detection of single molecules through SERS[29–31] despite the fact that the Raman effect is characteristically weak. Near-field microscopy based on SERS contrast has been reported.[32,33]

In pursuing apertureless NSOM or SERS, it is important for the experimentalist to have a quantitative understanding of the field enhancement for a given probe. This requires a means to calculate the field distributions around nanoscale objects excited by light. In the case of a plane wave interacting with a sphere, Mie scattering theory yields an analytical solution.[34] Analytical solutions are also available for other simple shapes, such as spheroids[35] or pairs of spheres.[36] It has been shown by Silva *et al.*[18] and Kalkbrenner *et al.*[37] that a single metal sphere isolated on the end of a glass tip can be used to generate subdiffraction limited images. However, the field enhancement for the sphere is much lower than for alternative geometries.[38] For more complex geometries, one has to rely on numerical simulations. It is possible to gain some insight by using static field calculations to solve the Laplace equations,[24] but significant errors arise when the size of the particle is large and field retardation become important. In order to properly treat the interaction of nanoparticles with optical fields, a full electromagnetic solution to the Maxwell's equations is needed.

There are several methods for numerically solving electromagnetism for any arbitrary geometry, such as the Green's function method,[39] the multiple multipole (MMP) technique,[40] and the finite difference time domain (FDTD) technique,[41] all of which have been applied to solve problems in near-field microscopy. While the MMP technique requires relatively little computational power, it requires a significant investment in user learning. The Green's function approach and FDTD require intensive computing power. Being more user friendly, with commercial software available, the finite difference time domain (FDTD) technique[41] has proved to be fruitful for solving near-field optical problems.[42–48] In this work, we take the FDTD approach to the design of optimal apertureless probes with strong field enhancement in the near-infrared regime. In this wavelength regime, it is possible to utilize two-photon fluorescence excitation, thus maximizing the contrast in the TENOM image.[23] Furthermore, near-infrared irradiation is more amenable to biological imaging than is visible excitation.

The rest of the paper is organized as follows: First, we describe analytical calculations for gold spheres and prolate spheroids. With these calculations, we illustrate the advantage of finite particles. Second, we discuss FDTD simulation of a gold sphere, and the verification of the accuracy of the FDTD technique via comparison of simulations to analytical solutions. Finally, we illustrate the FDTD design of field enhancing apertureless NSOM probes that are experimentally feasible. We simulate quasi-infinite and truncated conical probes, as well as right trigonal pyramids. Comparisons between these forms are made to find the optimal NSOM probe for use with near-IR excitation.

II. ANALYTICAL SOLUTION OF SCATTERING BY SPHEROIDAL GOLD PARTICLES

The optical properties of metals have been of interest for at least 100 years.[49] Gustav Mie provided the form of the solution to the problem of light scattering by spherical metal particles in 1908.[50] Other high-symmetry forms, including finite thickness slabs, cylinders, and ellipsoids, have been analytically solved.[35] These analytical solutions require only the particle size and frequency-dependent index of refraction, $\tilde{n}=n+ik$, with the real part representing the index of refraction and the imaginary part the extinction coefficient. These optical constants are available in the literature.[51]

For simple spheres, a separation of variables approach[35] allows calculation of the surface field intensity. With the excitation wavelength set at 825 nm, we used Mie scattering theory to determine the intensity enhancement available from the optimum sized sphere. The optical constants for the sphere were taken to be those of bulk gold, a good assumption for particles larger than tens of nm.[52] For smaller particles, the optical constants can be position dependent due to the additional damping by boundaries at the small scale. This is called a nonlocal effect, and can generate errors in field enhancement of up to 10% if left unaccounted.[53] Figure 1 shows the spectrum of intensity for the 210 nm sphere. We found that the maximum intensity enhancement at 825 nm excitation is a factor of ~21 with a sphere of diameter 210 nm. The maximum enhancement of ~22 actually occurs at 725 nm excitation. While larger enhancements are available with smaller spherical particles at shorter wavelengths (closer to the bulk plasma frequency),[54] ~22 is the highest possible intensity enhancement for a sphere excited with 825 nm light. This enhancement is insufficient for apertureless NSOM.

Prolate spheroids provide much higher intensity enhancements than do simple spheres, while remaining tractable by analytical calculations.[35] The surface intensity calculation for prolate spheroids is an extension of basic Mie scattering theory, expanding the scattered fields in terms of spherical functions. A *T*-matrix approach can be used to numerically evaluate the analytical solutions for cylindrically symmetric geometries.[35] In Fig. 2(a), we show the *T*-matrix calculated intensity enhancement at the ends of a prolate spheroid excited by 700 nm light polarized along the major axis. Here we vary the length of the semiminor axis of the particle. As the semiminor axis gets shorter for a given semimajor axis length, the spheroid ends become sharper. However, if the semiminor axis is too short, the excitation plane

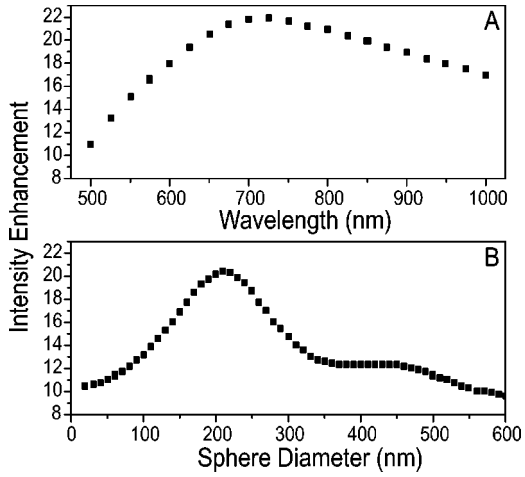

FIG. 1. Separation of variables solutions for a gold sphere excited in the near IR. The maximum surface intensity enhancement is plotted as a function of excitation wavelength for a 210 nm diameter sphere (a), and as a function of sphere diameter for spheres excited with 825 nm plane waves (b). The real and imaginary indices of refraction are from fitted experimental data. The field intensity distribution is measured in the plane of polarization of the incident wave, and the maximum enhancement at the surface is found. These plots indicate that, in the near-IR region, the maximum intensity enhancement for a sphere is on the order of 20.

wave will penetrate through the particle because of the finite skin depth of gold at optical frequencies (~60 nm at 700 nm excitation). For spheroids with semimajor axis lengths of 100 and 125 nm, the enhancement factor is highest for semiminor axis lengths of 23 and 29 nm, respectively. The peaks at the short end of the enhancement plot are a result of the optimum compromise between particle sharpness and skin depth induced transparency. These calculations provide an important insight regarding the enhancement of optical fields by sizable particles: sharper particles generate stronger fields.

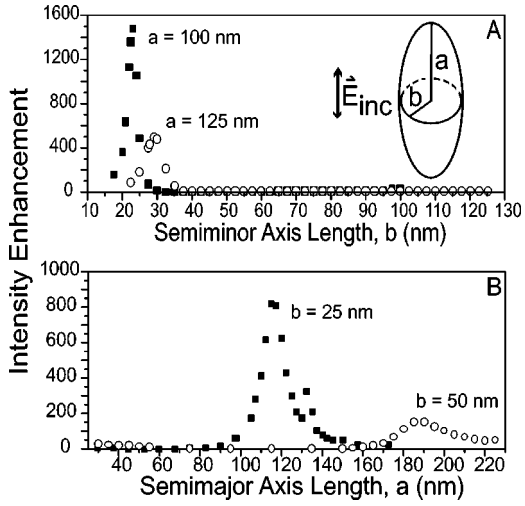

FIG. 2. Intensity enhancement at the ends of gold prolate spheroids. (a) The semiminor axis, b, is varied for particles with semimajor axis of $a=100$ and $a=125$ nm. The 700 nm excitation is polarized along the major axis of the spheroid, and the T-matrix method is used to calculate the external surface intensity. Strong resonances are seen for the narrower particle. (b) The semimajor axis, a, is varied for spheroids with semiminor axis lengths of $b=25$ and $b=50$ nm. The enhancement is sensitively dependent on the semimajor axis, and strong resonant lengths are observed.

This is akin to the static ''lightning rod'' effect, whereby charge accumulation at sharp points in metal objects results in strong fields.

However, the sharpness of the particle is not the entire story. In Fig. 2(b), we calculate the intensity enhancement for prolate spheroids with semiminor axes of both 25 and 50 nm, and varying semimajor axis lengths. A 230 nm long spheroid with semiminor axis of 25 nm has a strong intensity enhancement, ~815, that is roughly 40 times higher than that for a 345 nm long particle of the same girth, even though the longer particle is sharper. Similarly, the spheroid with semiminor axis length of 50 nm has a strong enhancement resonance at the semimajor axis length of 172.5 nm. There is a second, very sharp resonance for a 264 nm long particle with the 25 nm semiminor axis. Resonances as a function of semimajor axis length are known in the literature.[55] The spheroid acts as a resonant cavity that can only be driven efficiently when its size and fundamental surface plasmon resonance is matched to the excitation frequency. In order to utilize this physical picture for effective apertureless NSOM design, electromagnetic simulations of more complex geometries must be performed. The FDTD method provides a means of searching for optimal NSOM probes.

III. FDTD SIMULATION OF SPHERICAL GOLD PARTICLES

The finite difference time domain method is a flexible numerical means of solving electromagnetic problems by integrating Maxwell's differential equations,

$$\nabla\times\vec{E}+\mu_0\frac{\partial\vec{H}}{\partial t}=0,$$

$$\nabla\times\vec{H}-\frac{\partial\vec{D}}{\partial t}=0, \tag{1}$$

$$\vec{D}(t)=\varepsilon\varepsilon_0\vec{E}(t),$$

for an arbitrary geometry in three-dimensional space.[41,56] The space is divided into small units, typically cubes, called Yee cells.[57] This object definition mechanism is the heart of the flexibility of FDTD, as any arbitrary geometry can be simulated. Each cell is assigned the susceptibility for a given material. The FDTD method calculates the electric and magnetic fields in each cell by integrating the Maxwell's equations in a ''leap-frog'' fashion until the steady state is reached.[56] In the case of a sinusoidal excitation source, the steady state is reached when all scattered fields vary sinusoidally in time. The Mur absorbing boundary condition is used[58] at the sides of the simulated space.

In order to obtain an accurate field distribution for the three-dimensional object, the cell size must be much less than size of relevant features. In our case this requires a cell size of 3 nm. Such small cells result in extremely short time steps in the simulation, as the FDTD algorithm is stable only if $\Delta t\leqslant\Delta u/(c\sqrt{3})$, where u is the side of a cubical cell.[59] In order to reach the steady state of the problem, it is often necessary to subject the space to many optical cycles. This leads to simulations that run for tens of thousands of time steps. This precludes the use of smaller (e.g., 1.5 nm) cells

for the simulation of the probes. FDTD simulation is generally computationally intensive when high spatial precision is required. Fortunately, the recent rapid growth in available computational power has largely alleviated this problem. We use a commercial FDTD package (RemCom XFDTD 5.3) on a dual 1 GHz Pentium III computer.

Typically, FDTD calculations have been carried out for dielectric materials. Recent advances have extended the use of FDTD to the treatment of materials with frequency dependent, complex dielectric constants.[60] Real metals characteristically fall in this category. Leubbers *et al.* developed a FDTD algorithm for treating dispersive materials in a time-dependent fashion:[60]

$$\vec{D}(t)=\varepsilon_\infty\varepsilon_0\vec{E}(t)+\varepsilon_0\int_0^t\vec{E}(t-\tau)\hat{\chi}(\tau)d\tau. \tag{2}$$

Here, $\chi(\tau)$ is the Fourier transform of $\chi(\omega)$, and ε_0 is the permittivity of free space.

If the metal is assumed to follow the Drude model, one can derive the pertinent optical constants:

$$\begin{aligned}&\tilde{\varepsilon}=\varepsilon'+i\varepsilon'',\\&\varepsilon'=n^2-k^2,\\&\varepsilon''=2nk,\\&\tilde{\varepsilon}(\omega)=1+\frac{\omega_p^2}{\omega(i\nu_c-\omega)}=\varepsilon_\infty+\chi(\omega),\end{aligned} \tag{3}$$

where ε is the permittivity, χ is the susceptibility, ω is the angular frequency, ω_p is the radian plasma frequency, and ν_c is the collision frequency.

The Drude model is appealing in that it is derived from the simple physical picture of a free electron gas.[61] The response of near-field probes has been simulated under the Drude model using FDTD with some success.[42] However, the Drude model does not accurately describe the real and imaginary indices of refraction of noble metals over a wide frequency range. Also, the Fourier transform of $\chi(\omega)$ is often not numerically stable for the Drude model. In order to avoid problems with the Drude model, we instead approximate the experimentally determined optical constants of gold with a modified Debye function.[56] Modified Debye materials are described with equations containing a single pole:[56,62]

$$\tilde{\varepsilon}(\omega)=\varepsilon_\infty+\frac{\varepsilon_s-\varepsilon_\infty}{1+i\omega\tau}+\frac{\sigma}{i\omega\varepsilon_0}. \tag{4}$$

Here, ε_s represents the static permittivity, ε_∞ is the infinite frequency permittivity, σ is the conductivity, and τ is the relaxation time. The parameters are adjusted to closely match the experimentally observed optical properties. It is important to note that we associate little physical meaning to the individual parameters themselves, instead treating them as fitting constants to experimental results.

Under this model, we are able to obtain a good match over the near-infrared range of 700–1000 nm. (ε_s, ε_∞, σ, and τ are $-12\,987$, 9.012, 1.464×10^7 S/m, and 8.017×10^{-15} s, respectively.) This wavelength range covers the regime accessible to commonly available lasers, such as the Ti:Sapphire system or diode lasers. As such, probes designed for optimal use in this regime should be experimentally applicable for NSOM, particularly TENOM.

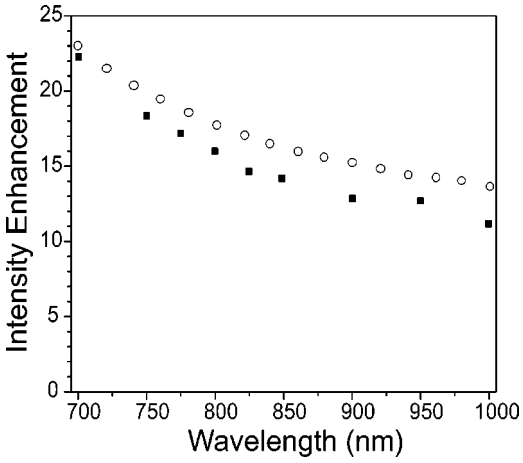

FIG. 3. The intensity enhancement for a 150 nm gold sphere is plotted as a function of wavelength. The intensity enhancement in the plane of polarization of the excitation plane wave is shown, and the maximum enhancement is normalized to the excitation intensity. The hollow circles are the separation of variables solution using the fitted experimental gold constants (Ref. 51) while the filled squares are the FDTD results using the modified Debye approximation.

In order to ensure the accuracy of the FDTD simulations using the fitted optical constants, the FDTD program was used to calculate the field strength in the equatorial plane of a 150 nm diameter ''sphere'' comprised of 3 nm cells in a 100 cell cubical space. The sphere was centered in the space, and all simulations were run for 12 000 time steps ($\Delta t=5.777$ as), sufficient for reaching steady state. Field distributions in the appropriate plane were collected every other time step during the last 600 time steps. At this time resolution, the optical cycle is comprised of ~240 data points. In Fig. 3, the maximum field intensity in each calculation was plotted as a function of wavelength, and we compared the results of an analytical Mie calculation[35] to those produced by the FDTD code. The FDTD code reproduces the analytical Mie theory remarkably well, particularly when one considers that there is some error in the match between the modified Debye model permittivities and the fitted experimental data. This verifies the validity of the FDTD simulation approach for design of gold probes.

IV. FDTD SIMULATION OF INFINITE AND TRUNCATED CONICAL GOLD PROBES

Apertureless NSOM experiments that have been reported in the literature[23] take advantage of the lightning rod effect by using gold tips that are well described as infinite cones with some defined end radius of curvature. These sharp conical tips are excited by light polarized at least partially along their long axes, and both theoretical and experimental work indicates strong intensity enhancement at the probe ends.[63,64]

While it is not possible to model truly infinite geometries using FDTD, we approximate the infinite geometry by cou-

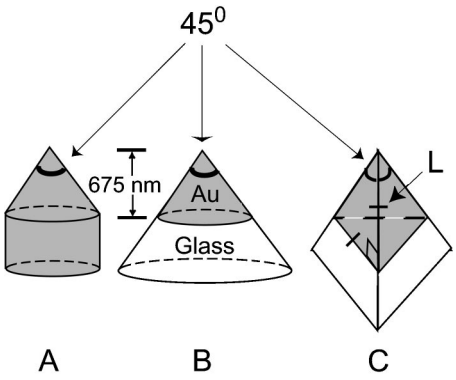

FIG. 4. Schematic representation of the three particles simulated in this work. (a), (b), and (c) are the quasi-infinite cone, the finite cone, and the right trigonal pyramid, respectively. The dimensions of interest are indicated on the images. In (c), the particle length "*L*" is the variable used to tune the particle size for optimum enhancement. In all cases, the Yee cell size is 3 nm. Each probe has a single cell point and a 45 degree angle of divergence. The glass permittivity in each case is set at 2.25.

pling a cylindrically symmetric gold tip to a perfectly conducting boundary condition. As shown in Fig. 4, the cone angle for the quasi-infinite tip is 45°, and the conical portion of the tip is 675 nm long. This conical section is terminated by a cylinder of gold, which is coupled to the boundary. While it would be preferable to simulate the probe as a cone diverging to the boundary of the space, this geometry results in unstable calculation due to the boundary conditions. Instabilities are alleviated when the metal surface is normal to the boundary. To simulate probes with ~10 nm end diameter, we use 3 nm cells. Each probe is terminated with a single 3 nm cell, which closely matches a probe with a 5 nm end radius of curvature. We observe no evidence of the single cell apex generating unrealistic field enhancements.

In Fig. 5(a), the tips are illuminated by 825 nm plane waves polarized along the axis of symmetry, and the field distribution across the center plane of the tip in the plane of propagation is recorded over the last 600 time steps. The maximum intensity enhancement, which occurs at the tip, is measured from these field images. At 825 nm excitation, the quasi-infinite probe yields an intensity enhancement of 361, similar to the intensity enhancement (196) simulated by finite element calculation for a 90° cone with a 10 nm radius hemispherical point.[63] We note that both our FDTD calculations and the finite element calculations of Martin *et al.* predict field enhancements lower than those of Novotny *et al.* from the MMP approach.[64]

Taking a cue from the prolate spheroid calculations discussed previously, we simulated the effect of truncating the quasi-infinite conical tip to a finite cone on a glass base as in Fig. 4(b). In Fig. 5(b), we show that a finite (675 nm long), 45° conical particle excited by 825 nm light yields an intensity enhancement factor of 918. Even though no size optimization has been attempted, this intensity enhancement is ~2.5× higher than that observed for the quasi-infinite conical tip. This improvement is despite the fact that the particle is presumably off resonance with the excitation source. The field distribution near the end of the finite cone is similar to the quasi-infinite cone, and therefore the achievable spatial

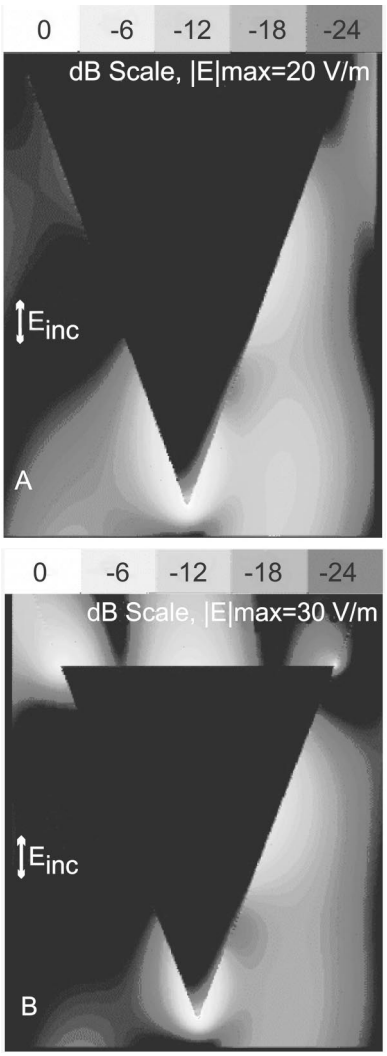

FIG. 5. FDTD simulated instantaneous electric-field magnitude distribution for conical tips excited by 1 V/m 825 nm light. The excitation polarization is indicated in the figure. (a) and (b) are the intensity distributions at peak intensity for the quasi-infinite [Fig. 4(a)] and finite conical [Fig. 4(b)] tips, respectively. Images are representative snapshots in time. The field distribution asymmetry is induced by the field propagation direction (left to right). The maximum intensity enhancement factor [361 for (a) and 918 for (b)] occurs immediately below the probe apex. This indicates the advantage of the finite geometry over the quasi-infinite tip for NSOM applications. Note that while the maximum field is higher for the truncated cone than for the quasi-infinite cone, the intensity distribution is qualitatively the same in each case.

resolution for both conical probes should be identical. This substantial improvement in enhancement factor can be achieved through use of finite probes in place of "infinite" tips.

V. FDTD SIMULATION OF PYRAMIDAL GOLD PROBES

We now explore the optimal shape for field enhancement. Jensen *et al.* observe strong, particle size tunable extinction spectra for arrays of truncated silver tetrahedra produced by nanosphere lithography, in accordance with discrete dipole approximation (DDA) calculations.[65] Jin *et al.* have recently produced small, triangular silver particles in the bulk through UV illumination of spherical colloidal spheroids, and DDA calculations predict their extinction-

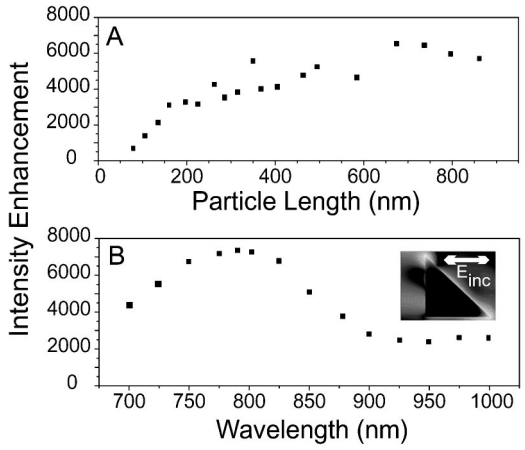

FIG. 6. FDTD calculated electric-field intensity enhancement as a function of particle length, L, and wavelength is plotted for the right trigonal pyramid [Fig. 4(c)]. The illumination polarization is indicated on the inset image. The direction of propagation of the incident wave is out of the plane of the image. The tip end of the probe is at the lower right of the image. (a) Is the size dependence of intensity enhancement for the right trigonal pyramid excited by 825 nm light. Due to computational constraints, the complete resonance is unobservable. In (b), however, the spectral resonance for the 675 nm long particle becomes clear. For both (a) and (b), the strongest enhancements occurs at the glass/gold interface opposite the particle right angle. The enhancements at the tip end are ~80% as large as the global maxima.

spectra.[66] In two-dimensional work, Kottmann *et al.* demonstrated that a triangle generates larger field enhancement than any of the other simulated simple shapes near the plasma frequency.[38] In contrast, we simulate larger, gold particles using the three-dimensional FDTD technique. These particles could easily be made using focused ion beam techniques, and we believe that the sharp edges present on these particles serve to collect charge and generate strong field enhancement.

We simulated the field enhancement generated by a three-dimensional right trigonal pyramid, as illustrated in Fig. 4(c). In Fig. 6(a), with excitation fixed at 825 nm light polarized along the tip axis, we varied the length of the particle arms to search for a resonance. For all simulations, the tip/boundary distance is 20 cells, while the gold/glass interface is 105 cells from the back boundary. The field intensities are recorded in the $X-Y$ plane containing the surface of the particle, and the maximum intensity enhancements in that plane are recorded. We were unable to observe the complete resonance curve in this fashion, as particles longer than ~875 nm are too large to be simulated due to computational constraints. In Fig. 6(b), we show the simulation of the spectral response of a 675 nm long particle in the 700 nm to 1000 nm window. In these simulations, an intensity enhancement resonance with excitation at 790 nm becomes clear. The intensity enhancement more than triples when tuning the excitation source from 1000 nm to 790 nm (up to ~7360 from ~2330). The spectral response of the asymmetrical particle, when considered alongside the comparison of finite to quasi-infinite conical probes, leads us to believe that longer pyramidal particles would yield lower enhancement factors.

The maximum intensity enhancement for the pyramidal geometry is 7360. In our simulations, this maximum enhancement occurs at the glass-gold junction. [See Fig. 4(c).] At the ''tip'' end of the particle, the enhancement is ~80% of the maximum value, though the introduction of a dielectric sample would likely increase this percentage to near the global maximum. The very ends of the pyramidal probes look similar to the conical probes. This is indicative of the importance of probe geometry beyond the immediate vicinity of the apex itself. The increase in enhancement when switching from conical to pyramidal probes is likely a result of the collection of charge at the sharp edges of the pyramid. Charge is driven to the tip end, resulting in large enhancement.

This enhancement factor is arguably the largest predicted for an NSOM probe realizable with today's technology. While Kottmann *et al.* have simulated two-dimensional particles with large enhancement factors, the extremely small size (20–50 nm) and sharpness (particle point radius of curvature = 0.25 nm) of these particles are prohibitive for fabrication and NSOM application. Our probe design not only provides large-field enhancement, but can be made with a modern focused ion beam.

In apertureless NSOM, the importance of large field enhancement is two-fold. First, it is preferable to have high-field enhancement to generate larger signal from the near-field region than from the far field being illuminated. For a linear signal response, this requires intensity enhancement of ~10 000 at the minimum. When two-photon fluorescence is employed, the contrast is substantially improved. The large intensity enhancement generated by our optimized probes should open the way for two-photon fluorescence or nonlinear Raman imaging at the size scale of membrane proteins. The second reason that high field enhancement is desirable is that strong enhancement allows the sample and the probe to be illuminated with much lower intensity light. (For practical reasons, the excitation source is passed through the sample via a high numerical aperture objective and focused on the probe.) Reducing the incident intensity should avoid photodamage to the sample. The use of optimal probes will therefore improve the overall durability of both the sample and the tip.

VI. CONCLUSIONS

The use of the apertureless NSOM probe as a strongly enhanced, localized excitation source for molecular transitions marks a substantial improvement in near-field microscopy. Not only does this method increase the spatial resolution of NSOM, but shifting the signal frequency away from the excitation frequency also makes image interpretation much simpler. In order to utilize these advantages, one must develop a probe with strong field enhancement. Electromagnetic simulations are paramount in this pursuit. Through the use of the modified Debye model,[56] we have demonstrated the capabilities of the FDTD method to accurately simulate the response of gold nanoparticles. Analytical calculations for scattering by prolate spheroids yield two important insights for the design of strongly enhancing probes: first, the enhancing probe must be sharp, and, second, the use of a

finite probe matched to the excitation source generates higher field enhancement. We have used FDTD calculations to demonstrate that this second insight applies to apertureless NSOM probes by calculating the advantage of the finite cone over the quasi-infinite conical tip in terms of field enhancement factors. The method presented above should serve as a guideline for designing alternative, finite, optimal apertureless NSOM probes.

By tailoring the shape, we have demonstrated that extremely large field enhancement should be possible far from the plasma frequency of gold. Furthermore, this strong field does not require any complex geometry, but can be generated by a simple particle amenable for use in apertureless NSOM. The intensity enhancement of right trigonal pyramid, of order 7400, should dramatically improve the use of apertureless NSOM. This enhancement occurs at an easily accessible 790 nm wavelength, and particles could, in principle, be tuned to a variety of near infrared laser sources. Furthermore, particles in this size and shape regime can be generated with FIB milling in a straightforward manner. With extremely strong field enhancement available, it should be possible to regularly achieve 10 nm spatial resolution. Such imaging capabilities open the door to high resolution optical studies of nanostructured materials and biologically interesting samples.

ACKNOWLEDGMENTS

The authors thank Lukas Novotny for helpful and stimulating discussions. This research was supported by the U.S. Department of Energy, Basic Energy Science Division. J.T.K.II received additional support from the Harvard University NIH Biophysical Training grant.

[1] E. H. Synge, Philos. Mag. **6**, 356 (1928).
[2] H. A. Bethe, Phys. Rev. Lett. **66**, 163 (1944).
[3] C. J. Bouwkamp, Philips Res. Rep. **5**, 321 (1950).
[4] E. A. Ash and G. Nicholls, Nature (London) **237**, 510 (1972).
[5] D. W. Pohl, W. Denk, and M. Lanz, Appl. Phys. Lett. **44**, 651 (1984).
[6] A. Harootunian, E. Betzig, M. Isaacson, and A. Lewis, Appl. Phys. Lett. **49**, 674 (1986).
[7] E. Betzig, J. K. Trautman, T. D. Harris, J. S. Weiner, and R. L. Kostelak, Science **251**, 1468 (1991).
[8] R. C. Dunn, Chem. Rev. **99**, 2891 (1999).
[9] V. Kurpas, M. Libenson, and G. Martsinovsky, Ultramicroscopy **61**, 187 (1995).
[10] B. I. Yakobson, A. LaRosa, H. D. Hallen, and M. A. Paesler, Ultramicroscopy **61**, 179 (1995).
[11] A. Lewis, M. Issacson, A. Harootunian, and A. Murray, Ultramicroscopy **13**, 227 (1984).
[12] J. D. McNeill, D. B. O'Connor, and P. F. Barbara, J. Chem. Phys. **112**, 7811 (2000).
[13] R. C. Dunn, G. R. Holtom, L. Mets, and X. S. Xie, J. Phys. Chem. **98**, 3094 (1994).
[14] M. Specht, J. D. Pedarnig, W. M. Heckl, and T. W. Haensch, Phys. Rev. Lett. **68**, 476 (1992).
[15] U. C. Fischer, J. Koglin, and H. Fuchs, J. Microsc. **176**, 231 (1994).
[16] S. Kawata and Y. Inouye, Ultramicroscopy **57**, 313 (1995).
[17] F. Zenhausern, Y. Martin, and H. K. Wickramasinghe, Science **269**, 1083 (1995).
[18] T. J. Silva, S. Schultz, and D. Weller, Appl. Phys. Lett. **65**, 658 (1994).
[19] A. Lahrech, R. Bachelot, P. Gleyzez, and A.C. Boccara, Opt. Lett. **21**, 1315 (1996).
[20] B. Knoll and F. Keilmann, Nature (London) **399**, 134 (1999).
[21] B. Hecht, H. Bielefeldt, Y. Inouye, and D. W. Pohl, J. Appl. Phys. **81**, 2492 (1997).
[22] L. Novotny, E. J. Sánchez, and X. S. Xie, Ultramicroscopy **71**, 21 (1998).
[23] E. J. Sánchez, L. Novotny, and X. S. Xie, Phys. Rev. Lett. **82**, 4014 (1999).
[24] W. Denk and D. W. Pohl, J. Vac. Sci. Technol. B **9**, 510 (1991).
[25] J. Jersch and K. Dickmann, Appl. Phys. Lett. **68**, 868 (1996).
[26] A. A. Gorbonuv and W. Pompe, Phys. Status Solidi A **145**, 333 (1994).
[27] F. W. King, R. P. Van Duyne, and G. S. Schatz, J. Chem. Phys. **69**, 4472 (1978).
[28] M. Moskovits, Rev. Mod. Phys. **57**, 783 (1985).
[29] S. Nie and S. R. Emory, Science **275**, 1102 (1997).
[30] K. Kneipp, Y. Wang, H. Kneipp, L. T. Perelman, I. Itzkan, R. R. Dasari, and M. S. Feld, Phys. Rev. Lett. **78**, 1667 (1997).
[31] A. M. Michaels, M. Nirmal, and L. E. Brus, J. Am. Chem. Soc. **121**, 9932 (1999).
[32] D. Zeisel, V. Deckert, R. Zenobi, and T. Vo-Dinh, Chem. Phys. Lett. **283**, 381 (1998).
[33] N. Hayazawa, Y. Inouye, Z. Sekkat, and S. Kawata, Opt. Commun. **183**, 333 (2000).
[34] M. Born and E. Wolf, *Principles of Optics*, 7th ed. (Cambridge University Press, Cambridge, UK, 1999).
[35] P. W. Barber and S. C. Hill, *Light Scattering by Particles: Computational Methods* (World Scientific, Singapore, 1990).
[36] M. Inouye and K. Ohtaka, J. Phys. Soc. Jpn. **52**, 3853 (1983).
[37] T. Kalkbrenner, M. Ramstein, J. Mlynek, and V. Sandoghdar, J. Microsc. **202**, 72 (2001).
[38] J. P. Kottman, O. J. F. Martin, D. R. Smith, and S. Schultz, Phys. Rev. B **64**, 235402 (2001).
[39] O. J. F. Martin, C. Girard, and A. Dereux, Phys. Rev. Lett. **74**, 526 (1995).
[40] C. Hafner, *The Generalized Multiple Multipole Technique for Computational Electromagnetics* (Artech, Boston, 1990).
[41] A. Taflove and M. E. Brodwin, IEEE Trans. Microwave Theory Tech. **23**, 623 (1975).
[42] R. X. Bian, R. C. Dunn, X. S. Xie, and P. T. Leung, Phys. Rev. Lett. **75**, 4772 (1995).
[43] D. Christensen, Ultramicroscopy **57**, 189 (1995).
[44] J. L. Kann, T. D. Milster, F. Froehlich, R. W. Ziolkowski, and J. Judkins, Ultramicroscopy **57**, 251 (1995).
[45] H. Nakamura, T. Sato, H. Kambe, K. Sawada, and T. Saiki, J. Microsc. **202**, 50 (2001).
[46] R. G. Milner and D. Richards, J. Microsc. **202**, 66 (2001).
[47] B. B. Akhremitchev, S. Pollack, and G. C. Walker, Langmuir **17**, 2774 (2001).
[48] H. Furukawa and S. Kawata, Opt. Commun. **148**, 221 (1998).
[49] P. Drude, Ann. Phys. (Leipzig) **1**, 566 (1900).
[50] G. Mie, Ann. Phys. (Leipzig) **25**, 377 (1908).
[51] P. B. Johnson and R. W. Christy, Phys. Rev. B **6**, 4370 (1972).
[52] D. S. Wang and M. Kerker, Phys. Rev. B **24**, 1777 (1981).
[53] P. T. Leung and W. S. Tse, Solid State Commun. **95**, 39 (1995).
[54] A. Wokaun, Mol. Phys. **56**, 1 (1985).
[55] E. J. Zeman and G. C. Schatz, J. Phys. Chem. **91**, 634 (1987).
[56] K. S. Kunz and R. J. Luebbers, *The Finite Difference Time Domain Method for Electromagnetics* (CRC, Boca Raton, FL, 1993).
[57] K. S. Yee, IEEE Trans. Antennas Propag. **14**, 302 (1966).
[58] G. Mur, IEEE Trans. Electromagn. Compat. **23**, 377 (1981).
[59] This is a result of the Courant stability condition, which has its basis in the fact that a plane wave traveling in the FDTD space must not travel through more than one cell in the space of a time step.
[60] R. J. Luebbers, F. Hunsberger, and K. S. Kunz, IEEE Trans. Antennas Propag. **39**, 29 (1991).
[61] N. W. Ashcroft and N. D. Mermin, *Solid State Physics* (W. B. Saunders, Philadelphia, 1976).
[62] R. J. Luebber, F. Hunsberger, K. S. Kunz, R. Standler, and M. Schneider, IEEE Trans. Electromagn. Compat. **32**, 222 (1990).
[63] Y. C. Martin, H. F. Hamann, and H. K. Wickramasinghe, J. Appl. Phys. **89**, 5774 (2001).
[64] L. Novotny, R. X. Bian, and X. S. Xie, Phys. Rev. Lett. **79**, 645 (1997).
[65] T. R. Jensen, G. C. Schatz, and R. P. Van Duyne, J. Phys. Chem. B **103**, 2394 (1999).
[66] R. Jin, Y. Cao, C. A. Mirkin, K. L. Kelly, G. C. Schatz, and Z. G. Zheng, Science **294**, 1901 (2001).